POLITECNICO DI TORINO
Repository ISTITUZIONALE

# Design and Verification of a Q-Band Test Source for UAV-Based Radiation Pattern Measurements

*Original*
Design and Verification of a Q-Band Test Source
for UAV-Based Radiation Pattern Measurements / Paonessa, F., Virone, G., Ciorba, L., Addamo, G., Lumia, M., Dassano, G., Zannoni, M., Franceschet, C., Peverini, O.A.. - In: IEEE TRANSACTIONS ON INSTRUMENTATION AND MEASUREMENT. - ISSN 0018-9456. - ELETTRONICO. - 69:12(2020), pp. 9366-9370. [10.1109/TIM.2020.3031127]

*Availability:*
This version is available at: 11583/2920534 since: 2021-09-21T14:30:51Z

*Publisher:*
IEEE

*Published*
DOI:10.1109/TIM.2020.3031127

*Terms of use:*

This article is made available under terms and conditions as specified in the corresponding bibliographic description in the repository

*Publisher copyright*
IEEE postprint/Author's Accepted Manuscript

©2020 IEEE. Personal use of this material is permitted. Permission from IEEE must be obtained for all other uses, in any current or future media, including reprinting/republishing this material for advertising or promotional purposes, creating new collecting works, for resale or lists, or reuse of any copyrighted component of this work in other works.

(Article begins on next page)

14 November 2026

# Design and Verification of a Q-Band Test-Source for UAV-Based Radiation Pattern Measurements

Fabio Paonessa, Giuseppe Virone, Lorenzo Ciorba, Giuseppe Addamo, Mauro Lumia, Gianluca Dassano, Mario Zannoni, Cristian Franceschet, and Oscar A. Peverini

***Abstract*—In the last years, the Unmanned Aerial Vehicles (UAVs) generated significant innovations in in-situ antenna measurements. UAV-mounted test sources have been exploited to characterize the radiation pattern of receiving antennas and arrays for HF radars, radio telescopes in VHF band, and up to the X-band for radar characterization. A UAV test source operating in the Q-band has been recently developed within the Large-Scale Polarization Explorer (LSPE) project. It will be used for the in-situ validation of a ground-based cluster of coherent polarimeters for cosmology observation. This paper presents the payload solution that is actually applicable to general UAV-based radiation pattern measurements in the Q-band. It is based on Phase Locked Loop synthesizer and an active multiplier coupled with a power detector to compensate for signal power drifts in post-processing. Relevant system tests have been performed in both laboratory environment and operative conditions. The measured outdoor radiation patterns are in good agreement with both anechoic chamber measurements and simulated data.**

***Index Terms*—antenna measurements, radiation pattern, unmanned aerial vehicles.**

## I. Introduction

The Unmanned Aerial Vehicles (UAVs) technology produced one of the most significant innovations for in-situ antenna measurements in the last decade. UAVs equipped with RF transmitters have been initially used for the characterization of HF radars [1] and VHF radio astronomical antennas and arrays [2-4]. UAV-based systems in transmit mode have been also used in the L-band [5] and X-band [6]. Receive mode payloads have been developed in [7].

This paper presents a Q-band payload solution for in-situ UAV-based radiation pattern measurements in transmit mode. It has been originally developed in the framework of the Large-Scale Polarization Explorer (LSPE) [8], where it will be used to characterize the radiation patterns of the LSPE Strip instrument. Strip is a ground-based installation featuring a cluster of Q-band coherent polarimeters [9] aimed at measuring the B-modes of the polarized cosmic microwave background. Besides radiation patterns, polarization characterization will be also considered [10].

The paper is organized as follows: the airborne Q-band payload is described in Section 2, whereas Section 3 presents the results of the experimental test, in which the *E*-plane of a smooth wall circular horn is measured at 44 GHz with the proposed UAV system and compared to both simulation data and indoor measurements in anechoic chamber.

## II. Q-Band Payload

### A. RF generator

The proposed solution aims at covering the whole Q-band (33-50 GHz) by means of a Phase Locked Loop (PLL) frequency synthesizer and an active frequency multiplier. Fig. 1a shows the present implementation, which is based on a Valon Technology 5015 synthesizer (1) [11], featuring a PLL with integrated voltage-controlled oscillator with maximum output frequency of 15 GHz, and a Sage Millimeter SFA series frequency multiplier (2) [12]. The multiplier (2) WR-22 rectangular waveguide output is connected to a directional coupler (3) (Sage Millimeter SWD series

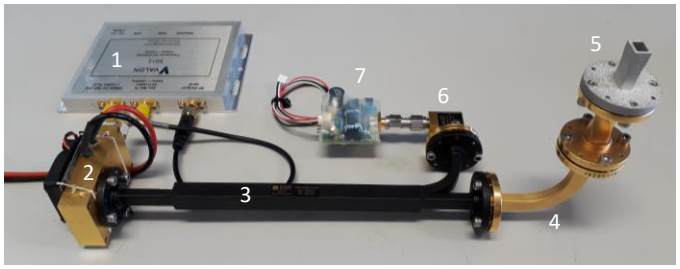


(a)

(b)

Fig. 1. (a) The Q-band payload composed of: frequency synthesizer (1), active multiplier (2), directional coupler (3), bend and twist (4), rectangular horn (5), amplitude detector (6) and precision voltage amplifier (7). (b) The payload mounted on the UAV.

Manuscript received July xx, 2020. This work was partially supported by the Italian Space Agency (ASI) in the framework of Contract I/022/11/0 entitled "Large Scale Polarization Explorer (LSPE)."

F. Paonessa, G. Virone, L. Ciorba, G. Addamo, M. Lumia and O. A. Peverini are with the Italian National Research Council (CNR), Institute of Electronics, Computer and Telecommunication Engineering (IEIIT), 10129 Turin, Italy (e-mail: fabio.paonessa@ieiit.cnr.it; giuseppe.virone@ieiit.cnr.it; lorenzo.ciorba@ieiit.cnr.it; giuseppe.addamo@ieiit.cnr.it; mauro.lumia@ieiit.cnr.it; oscar.peverini@ieiit.cnr.it).

G. Dassano is with Polytechnic of Turin, Department of Electronics and Telecommunications (DET), 10129 Turin, Italy (email: gianluca.dassano@polito.it).

M. Zannoni is with University of Milan-Bicocca, Department of Physics, 20126 Milan, Italy (email: mario.zannoni@unimib.it).

C. Franceschet is with University of Milan-Celoria, Department of Physics, 20133 Milan, Italy (email: cristian.franceschet@fisica.unimi.it).

[13]). The direct port of the coupler connects an 8-dBi-gain rectangular horn (5) through an *E*-plane bend and twist (4). The horn has been manufactured through the selective laser melting process of [14, 15] and is pointed toward the nadir when mounted on the UAV (see Fig. 1b). The coupled port (-30 dB) is connected to a diode-based amplitude detector (6) (Sage Millimeter SFD [16]) and a precision voltage amplifier (7) to measure possible in-flight variations of the generated power as described in section II.B. The total weight of the designed payload is about 600 g.

The main advantages of the adopted PLL-based configuration with respect to mechanically tuned Gunn-diode oscillators (*e.g.*, Sage SOM series, [17]) are the superior frequency accuracy (±2 ppm) and lock time (<100 µs) [11]. Moreover, Gunn oscillators in Q-band have a temperature coefficient of about -3 MHz/°C, which potentially causes a long settling period and significant frequency fluctuations in flight. The PLL frequency stability is instead within ±0.5 ppm from -20 °C to +70 °C of case temperature, which corresponds to less than 70 Hz/°C at 12.5 GHz of output frequency.

It has been found that the strong vibrations produced by the UAV motors can generate a spurious modulation of the RF signal. A specific indoor test has been conceived with the UAV fastened to the floor and its motors spinning at variable speed. A spectrum analyzer (Anritsu MS2760A) acquired the signal at the output of the multiplier. According to Fig. 2, the maximum measured spread from the lock frequency was ±35 kHz (±0.875 ppm) with a rigid flange (red dotted curve) and ±10 kHz (±0.25 ppm) with a custom-built damping flange (yellow dash-dotted curve). For comparison, similar tests with the Gunn oscillator showed up to ±10 MHz (±200 ppm) in undamped condition.

The observed spurious modulation is relevant for radiation pattern measurements where a narrow band receiver (e.g. spectrum analyzer in span zero mode) is generally adopted. It is worth mentioning that the sum of the frequency accuracy and the vibration-induced modulation must fit within the receiver bandwidth. The test results in Fig. 2 and Fig. 3 show that a bandwidth of 1 MHz is sufficient. In Fig. 3, the differences between the two spectrum analyzer traces acquired in span zero mode with motors off (black solid curve) and at max. speed (gray dotted curve) are negligible.

### *B. Amplitude detector and precision voltage amplifier*

Thermal variations will likely occur in flight due to the variable airflow and weather conditions even if proper active dissipation has been implemented. In the developed payload, the most critical device is the active multiplier. Laboratory tests under different conditions of heat dissipation highlighted up to 5 dB of power drop at the output of the multiplier during a warm-up period of 30 minutes. Besides the unpractical transient duration, such variations would produce an evident distortion in the measured radiation patterns. For this reason, the designed payload features an amplitude detector to measure such fluctuations of the RF power during the flight. The WR-22 detector input is connected to the coupled port, whereas the coaxial analog output port is connected to the Analog-to-Digital Converter (ADC) pin of the flight controller (pixhawk) [18] by means of a precision voltage amplifier. In this way, the recorded data can be easily used in post processing as they are logged with the same GPS timestamp of the UAV position and attitude data.

The precision voltage amplifier consists of a custom circuit featuring a double-stage low-offset amplifier, having a measurement dynamic of about 6 dB and a gain error within 1%, *i.e.*, about 0.09 dB (verified with an HP 3478A digital multimeter).

The accuracy of the amplitude detector readings has been verified in laboratory at three different frequencies. The digitized output voltage of the amplitude detector and the signal power at the output of the direct port (through a spectrum analyzer) have been measured during a warm-up period of 30 minutes. Fig. 4 shows the calibrated response of the device. The agreement between the readings of the measurement setups is within 0.05 dB.

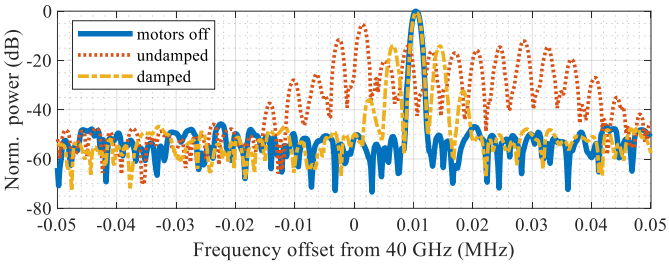


Fig. 2. Acquired spectra at the output of the multiplier (bandwidth 1 kHz). Motors off (blue solid); motors at max. speed with rigid flange (red dotted) and damped flange (yellow dash-dotted). The curves are normalized to the peak power with motors off. The preset PLL frequency was 10 GHz (40 GHz after the multiplier).

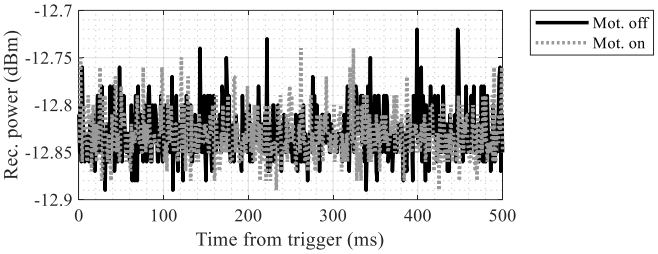


Fig. 3. Test-acquisitions with the spectrum analyzer, in zero-span mode and RBW = 1 MHz. Motors off (black solid), motors at max. speed (gray dotted).

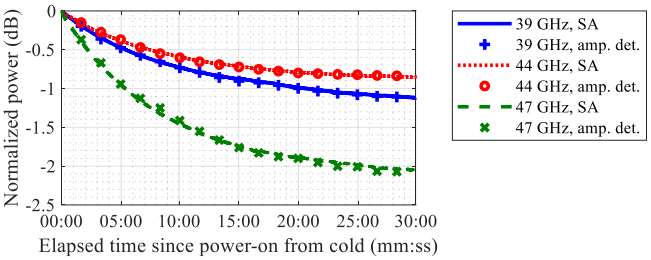


Fig. 4. Comparison between the amplitude detector readings (markers) and the spectrum analyzer measurements (lines), during a warm-up period of 30 minutes at three different frequencies: 39 GHz (blue), 44 GHz (red) and 47 GHz (green). Curves normalized to their initial value.

## III. Outdoor System Test

### *A. Outdoor experimental setup*

The system has been tested outdoor on a 23-dB-gain smooth wall circular horn [14]. The horn was placed on a 1.8 m tripod on the measurement field, pointed toward the zenith. It was connected to a circular-to-rectangular waveguide transition and a 30-dB Low Noise Amplifier (LNA) (Sage Millimeter SBL series). An Anritsu MS2760A spectrum analyzer was connected to the LNA through a 2.4-mm cable and a waveguide-to-coaxial transition. The PPS signal from an external GPS receiver triggered the analyzer at 1-Hz rate. The analyzer was configured in span-zero mode and 1 MHz resolution bandwidth (see section II.A).

The Q-band payload was accommodated in a commercial 3D Robotics X8+ octocopter (see Fig. 1b). The planned path consisted in

a rectilinear constant-height flight at 20-m height lying in the *E*-plane of the circular horn. The multicopter was equipped with a real-time differential GPS that provided centimeter-level accurate position data and allowed the UAV to follow the planned path within 20 cm of displacement, which corresponds to less than 0.6° deviation from the ideal *E*-plane.

The measured pattern is computed from the received power according to [19] (based on the Friis equation under the far-field approximation). In this experiment, however, the transmitted power is a measured quantity that varies during the flight. The centimeter-level position accuracy produces a knowledge error of about 0.05° in the scan angle and 0.02 dB in the measured pattern.

As far as the accuracy of the relative orientation between the UAV and the Antenna Under Test (AUT) is concerned, the measured UAV attitude (i.e. the three orientation angles: yaw, pitch and roll [20]) is generally accurate within ±2°. The effect of the attitude uncertainty on the performance of polarization measurements can be evaluated directly in the principal planes: letting δα be the orientation error between UAV and AUT E-planes (mainly related to yaw error), the co-polar component of the incident electric field on the AUT is proportional to cos(δα), whereas the cross-polar component is proportional to sin(δα) [21]. Therefore, an uncertainty of ±2° produces an error of about -0.005 dB in the measured co-polar level and a spurious cross-polar level of about -29 dB.

### B. Results

The results are reported in Fig. 5: the outdoor-measured *E*-plane pattern (blue dot-dashed curve) at 44 GHz is shown along with the indoor measurement in anechoic chamber (red dashed curve) and the simulated *E*-plane curve (black dotted curve). The simulated curve has been computed using a coupled integral equation formulation [22].

In Fig. 5, the curves are normalized to their maximum value, i.e. at $\theta = 0°$. The overall consistency is remarkable. According to [23], the weighted logarithmic difference has been adopted as figure-of-merit for both the outdoor measurement and the indoor one, with respect to the simulation. The simulated *E*-plane pattern is used as weighting function, with $\beta = 0.5$. The good agreement between the data is confirmed by the RMS of the weighted logarithmic difference, which is 0.108 dB for the chamber measurement and 0.153 dB for the outdoor one. For the outdoor measurement, errors can be explained by the uncertainty of both the on-ground circular horn orientation and the UAV attitude data [20].

A small transmitted power reduction of 0.5 dB has been recorded during the flight thanks to optimal weather conditions (light breeze) and the short scan duration (20 s). However, it should be noted that such a small variation is higher than the final figure-of-merit obtained above (0.153 dB RMS). This confirms the benefit from the implemented power measurement scheme and its exploitation in the data post-processing.

## IV. Conclusion

A payload solution for in-situ UAV-based radiation pattern measurements in Q-band has been proposed. The design addressed the main critical issues related to the application, in particular the frequency instability due to both thermal variations and motor vibrations and the compensation for the output power fluctuations. An outdoor measurement at 44 GHz on a circular horn has been compared to both simulation data and anechoic chamber measurements showing remarkable agreement.

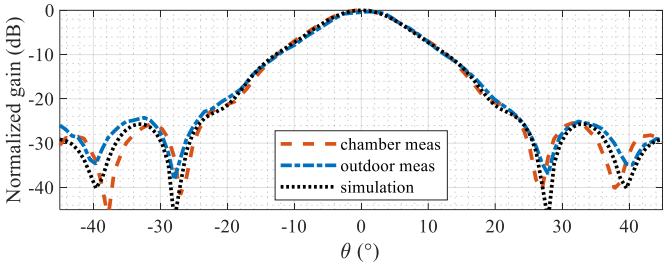


Fig. 5. Comparison of the measured *E*-plane patterns for the reference horn at 44 GHz. Red dashed curve: indoor measurement. Blue dot-dashed curve: UAV-based outdoor measurement. Black dotted curve: simulated pattern.

## Acknowledgment

The authors would like to express their recognition to Dr. Flaviana Calignano (DIGEP, Polytechnic of Turin) for providing the additively manufactured horn.

## References

[1] L. Washburn, E. Romero, C. Johnson, C. Gotschalk and B. Emery, "Antenna calibration for oceanographic radars using aerial drones," in *2016 IEEE Conference on Antenna Measurements & Applications (CAMA)*, Syracuse, NY, 2016, pp. 1-4

[2] G. Virone *et al.*, "Antenna Pattern Verification System Based on a Micro Unmanned Aerial Vehicle (UAV)," in *IEEE Antennas and Wireless Propagation Letters*, vol. 13, pp. 169-172, 2014

[3] G. Virone *et al.*, "Strong Mutual Coupling Effects on LOFAR: Modeling and In Situ Validation," in *IEEE Transactions on Antennas and Propagation*, vol. 66, no. 5, pp. 2581-2588, May 2018

[4] P. Bolli *et al.*, "Near-Field Experimental Verification of the EM Models for the LOFAR Radio Telescope," in *IEEE Antennas and Wireless Propagation Letters*, vol. 17, no. 4, pp. 613-616, April 2018

[5] I. Farhat, D. Cutajar, M. Bezzina and K. Z. Adami, "Drone Characterization Approach for Radio Telescopes," in *2019 PhotonIcs & Electromagnetics Research Symposium - Spring (PIERS-Spring)*, Rome, Italy, 2019, pp. 3016-3018

[6] S. Duthoit *et al.*, "A new approach for in-situ antenna characterization, radome inspection and radar calibration, using an Unmanned Aircraft System (UAS)," in *2017 IEEE Radar Conference (RadarConf)*, Seattle, WA, 2017, pp. 0669-0674

[7] M. García-Fernández *et al.*, "Antenna Diagnostics and Characterization Using Unmanned Aerial Vehicles," in *IEEE Access*, vol. 5, pp. 23563-23575, 2017

[8] L. Lamagna *et al.*, "Progress Report on the Large-Scale Polarization Explorer", in *Journal of Low Temperature Physics*, Apr. 2020

[9] C. Franceschet, *et al.*, "The STRIP instrument of the Large Scale Polarization Explorer: Microwave eyes to map the Galactic polarized foregrounds," in *Proceedings of SPIE*, vol. 10708, 2018

[10] F. Nati *et al.*, "POLOCALC: a Novel Method to Measure the Absolute Polarization Orientation of the Cosmic Microwave Background," in *Journal of Astronomical Instrumentation*, Vol. 6, No. 2, 2017

[11] Valon Technology, LLC. 5015 Synthesizer Specifications. [Online]. Available: https://www.valonrf.com/uploads/1/1/7/3/117370920/valon_5015_synthesizer_specifications_sr_20180531.pdf. Accessed on: Sept. 16, 2020

[12] Eravant (formerly SAGE Millimeter). SFA-224SF-S1 datasheet. [Online]. Available: https://sftp.eravant.com/content/datasheets/SFA-224SF-S1.pdf. Accessed on: Sept. 16, 2020

[13] Eravant (formerly SAGE Millimeter). SWD-3030E-22-SW datasheet. [Online]. Available: https://sftp.eravant.com/content/datasheets/SWD-3030E-22-SW.pdf. Accessed on: Sept. 16, 2020

[14] G. Addamo *et al.*, "3-D Printing of High-Performance Feed Horns From Ku- to V-Bands," in *IEEE Antennas and Wireless Propagation Letters*, vol. 17, no. 11, pp. 2036-2040, Nov. 2018

[15] G. Addamo *et al.*, "Additive Manufacturing of Ka-Band Dual-Polarization Waveguide Components," in *IEEE Trans. Microw. Theory Tech.*, vol. 66, no. 8, pp. 3589-3596, Aug. 2018

[16] Eravant (formerly SAGE Millimeter). SFD-333503-22SF-P1 datasheet. [Online]. Available: https://sftp.eravant.com/content/datasheets/SFD-333503-22SF-P1.pdf. Accessed on: Sept. 16, 2020

[17] SAGE Millimeter. Mechanically Tuned Gunn Oscillators, SOM Series, Electrical Specifications. [Online]. Available: https://www.amtechs.co.jp/product/Mech.pdf. Accessed on: Sept. 16, 2020

[18] Ardupilot Documentation, Pixhawk Overview. [Online]. Available: https://ardupilot.org/copter/docs/common-pixhawk-overview.html. Accessed on: Sept. 16, 2020

[19] G. Virone *et al.*, "Antenna pattern measurements with a flying far-field source (Hexacopter)," in *2014 IEEE Conference on Antenna Measurements & Applications (CAMA)*, Antibes Juan-les-Pins, 2014, pp. 1-2

[20] F. Paonessa *et al.*, "Effect of the UAV orientation in antenna pattern measurements," in *2015 9th European Conference on Antennas and Propagation (EuCAP)*, Lisbon, 2015, pp. 1-2

[21] G. Virone *et al.*, "UAV-based technique for the characterization of the Intrinsic Cross-Polarization Ratio (IXR)," in *2017 11th European Conference on Antennas and Propagation (EUCAP)*, Paris, 2017, pp. 3825-3828

[22] G. Addamo, O. A. Peverini, G. Virone, R. Tascone and R. Orta, "Model-Order Reduction Technique for the Efficient Analysis of Complex Waveguide Structures. An Application to the Design of Corrugated Horns," in *IEEE Antennas and Wireless Propagation Letters*, vol. 8, pp. 1039-1042, 2009

[23] S. Pivnenko *et al.*, "Comparison of Antenna Measurement Facilities With the DTU-ESA 12 GHz Validation Standard Antenna Within the EU Antenna Centre of Excellence," in *IEEE Transactions on Antennas and Propagation*, vol. 57, no. 7, pp. 1863-1878, July 2009